Research Article Vol. 31, No. 2 / 16 Jan 2023 / Optics Express 843
Optics EXPRESS

# Time-expanded φOTDR using low-frequency electronics

MIGUEL SORIANO-AMAT,[1] HUGO F. MARTINS,[2] SONIA MARTIN-LOPEZ,[1] MIGUEL GONZALEZ-HERRAEZ,[1] MARÍA R. FERNÁNDEZ-RUIZ,[1] AND VICENTE DURÁN[3,*]

[1] *Universidad de Alcalá, EPS, 28805 Madrid, España, Spain*
[2] *Instituto de Óptica "Daza de Valdés" IO-CSIC, C/Serrano 121, 28006 Madrid, Spain*
[3] *Institute of New Imaging Technologies, GROC-UJI, 12071, Castellón, Spain*
[*] *vduran@uji.es*

**Abstract:** Time expanded phase-sensitive optical time-domain reflectometry (TE-φOTDR) is a recently reported technique for distributed optical fiber sensing based on the interference of two mutually coherent optical frequency combs. This approach enables distributed acoustic sensing with centimeter resolution while keeping the detection bandwidth in the megahertz range. In this paper, we demonstrate that TE-φOTDR can be realized with low-frequency electronics for both signal generation and detection. This achievement is possible thanks to the use of a couple of electro-optic comb generators driven by commercially available step recovery diodes. These components are fed by radio frequencies that are orders of magnitude lower than those involved in the signals so far originated by ultrafast waveform generation. The result is a simple, compact, low-cost and potentially field-deployable sensor that works without resorting to any decoding algorithm. Besides, high-resolution distributed sensing is carried out with no need of coding strategies or enhanced backscatter fibers. To check the capabilities of our system, we perform distributed strain sensing over a range of 20 m. The spatial resolution is 3 cm and the acoustic sampling rate can be increased up to 200 Hz. This performance reveals the prospective of the proposed approach for field applications, including structural health monitoring.



## 1. Introduction

Phase-sensitive (φ)OTDR is a technique that exploits the coherence of narrow linewidth laser sources to perform real-time distributed acoustic sensing (DAS) [1–3]. In conventional schemes, φOTDR makes use of coherent pulses that propagate along a sensing fiber, originating a return signal as a consequence of Rayleigh scattering. This backscattered signal, albeit very weak, is sensitive to phase changes induced by dynamic temperature and strain perturbations occurring along the fiber. By detecting and analyzing the backscattered signal, these perturbations can be precisely measured and localized. In φOTDR, the pulse width determines the attainable range resolution, so short pulses providing high resolutions involve ultrafast photodetectors. In addition, when long sensing distances are considered, the need of injecting high peak-power pulses into the fiber can provoke the onset of nonlinear effects. This drawback can be avoided by employing coded pulse sequences, although at the cost of resorting to complex decoding algorithms [4,5].

Recently, we have proposed a novel sensing approach called time expanded (TE-)φOTDR, which is able to provide centimeter resolutions with detection electronics in the megahertz range [6]. The operation principle relies on the electro-optic (EO) generation of two mutually coherent optical frequency combs (OFCs) from a continuous-wave (cw) laser, each one with different line spacing. In this dual-comb scheme, one comb (the probe) interrogates the sensing fiber, while the other comb (the local oscillator, LO) interferes with the signal that is backscattered from the fiber. In the frequency domain, this interference leads to a multi-heterodyne detection process, so the generated optical spectra can be mapped into a very narrow radio-frequency (RF) region [7].

#475541 https://doi.org/10.1364/OE.475541
Journal © 2023 Received 13 Sep 2022; revised 15 Nov 2022; accepted 5 Dec 2022; published 3 Jan 2023

Optics EXPRESS

In the time domain, the detection of the interference between the probe and the LO originates, after a low-pass filtering process, a cross-correlation signal extending over a time interval equal to the inverse of the difference in the line spacing of the combs. Therefore, the duration of an interferogram (IGM) is orders of magnitude longer than the period of the combs. By analyzing the phase of a sequence of recovered time signals, temperature and strain perturbations can be dynamically measured, with a spatial resolution and an acoustic sampling rate that depend on the parameters of the designed combs.

In previous demonstrations of TE-φOTDR, an arbitrary waveform generator (AWG) was used to drive a couple of EO intensity modulators by means of tailored electrical signals [6,8]. In this scheme, the EO modulation results in the creation of two OFCs, each one composed of two bands extending over several gigahertz. By optically filtering one of these bands, an unambiguous frequency down-conversion is ensured. The AWG enables a precise selection of the spectral phase of the combs and, hence, a control of the temporal shape of the probe and the LO. Specifically, limiting the light peak power serves to optimize the signal-to-noise ratio (SNR) of the backscattered signal, as well as to avoid the onset of nonlinearities [8]. This control of the spectral phase, combined with the generation of OFCs with very dissimilar line spacing, makes it possible real-time sensing over kilometer distances, while preserving centimeter resolution and megahertz detection [6]. However, all these benefits are achieved with the aid of a high-performance AWG operating at sampling rates of tens of gigahertz. Alternatively, the AWG can be replaced by two pseudorandom bit sequence generators driven by gigahertz-frequency signals, which must be produced with hertz-level precision [9]. This second scheme enables temperature sensing over distances of a few hundred meters with centimeter resolution and acoustic sampling rates of several hertz. Despite all these developments, performing TE-φOTDR using low-frequency electronics (not only for the signal detection but also for the comb generation) is challenging and so far has remained unexplored. In particular, it implies the creation of two ultra-dense OFCs covering a few gigahertz of bandwidth (to ensure centimeter resolutions) by employing electronics in the megahertz range. The interfering combs, besides showing a high mutual coherence, need to be generated in such a way that they lead to an unambiguous RF spectrum. Achieving these requirements without sophisticating the optical setup represents a significant step to facilitate the use of TE-φOTDR in a variety of practical applications.

In this paper, we tackle the above question and propose a TE-φOTDR scheme that can reduce the frequency of the RF signals for dual-comb generation by three orders of magnitude, while keeping a very low sampling rate at the detection stage. This is possible by creating OFCs from a couple of EO modulators driven by step recovery diodes (SRDs). These diodes are passive, hands-free components that can transform a single-tone RF signal into a train of short electrical pulses, with a repetition rate equal to the input RF frequency [10,11]. SRDs have been already employed to produce picosecond pulses using low-driving-voltage EO modulators [12], OFCs by gain-switching of semiconductor lasers [13] and a couple of EO-OFCs for dual-comb molecular spectroscopy [14]. In the latter application, mutually coherent OFCs with a line spacing of ≃200 MHz covering >50 GHz have been demonstrated. If applied to TE-φOTDR, OFCs must be scaled down. Specifically, SRDs are required, as mentioned before, to produce ultra-dense combs with sufficiently wide bandwidth to guarantee centimeter resolution over ranges of tens of meters. This performance is indeed achieved by some SRD-based pulse generators at a very reduced cost (~0.1 k€), as we shall show in the next section [15]. In addition, the dual-comb approach that we propose includes an acousto-optic frequency shifter (AOFS) to guarantee a frequency-down conversion without aliasing. This solution, widely utilized in dual EO comb interferometry [16], avoids filtering out half of the generated optical comb spectra (with the subsequent reduction of the spatial resolution) and only requires RF signals of tens of megahertz. The price to pay for all these advantages is a limitation on the attainable sensing range (up to a few tens of meters), due to the use of pulses in both the electrical and optical domains. However,

Optics EXPRESS

fast and precise sensing over such distances has a great potential for structural health monitoring in civil and aerospace applications [17–19].

## 2. Dual-comb scheme for TE-ΦOTDR

### 2.1. Description of the setup

The setup employed in our experiments is shown in Fig. 1. As a light source, we employ a continuous-wave laser (CWL) with a linewidth <0.1 kHz and a thermal tuning range of 1 nm around $\nu_0$ = 1545 nm (NKT Koheras Basik E15). The laser light is divided into two arms (the probe and the LO) by a 10 dB coupler, which sends 90% of the light to the LO. In each path, the laser light goes through a Mach-Zehnder modulator (MZM) driven by a SRD (TBCG2 from Tekbox) [15]. The pulse repetition rates for the probe and the LO are, respectively, $f_r$ and $f_r + \delta f$ ($\delta f \ll f_r$). These frequencies are produced using a two-channel RF generator (Gen.). The MZMs are biased at their zero transmission point and fed by electrical pulses with an amplitude of around the modulators' half-wave voltage, $V_\pi$ (≅5 V). In the probe arm, the optical signal is amplified by an erbium-doped fiber amplifier (EDFA) up to ~200 mW. The emerging light is then filtered by a fiber Bragg grating (FBG) with a bandwidth (BW) of 0.37 nm. By means of a circulator, the resulting signal propagates along the fiber under test (FUT), which is mechanically perturbed by a shaker over an adjustable perturbation length (PL). The probe's repetition rate $f_r$ must be set in accordance to the total length $L$ of the FUT, such that $f_r \leq c/(2nL)$, where $c$ is the speed of light in a vacuum and $n$ is the fiber refractive index. The weak backscattered signal generated by the FUT is amplified by a second EDFA and optically filtered by another FBG (with a BW of 0.11 nm). In the LO arm, an acousto-optic frequency shifter (AOFS) is placed before the MZM to ensure a non-ambiguous frequency down-conversion, as explained below. The LO comb is made to interfere with the probe backscattered signal. A polarization controller and two variable optical attenuators (VOAs) are placed before the last coupler to maximize the interference signal, which is measured with a balanced photodetector (BPD). The electrical signal originated upon detection passes through a low-pass filter (LPF) and is digitized by an oscilloscope (Osc.). The AOFS driver, the SRD signals and the oscilloscope are locked to the same reference clock.

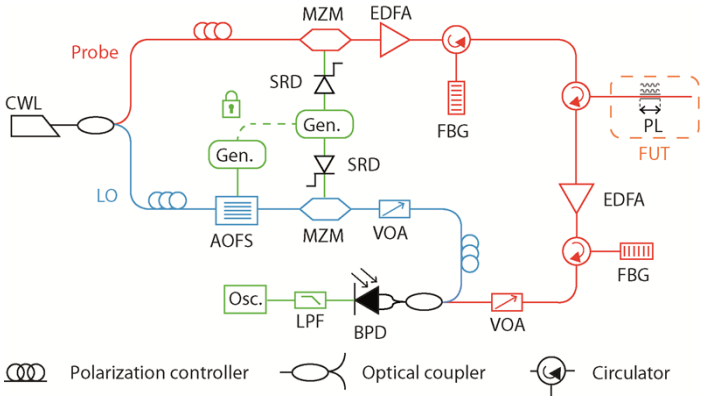


**Fig. 1.** Experimental setup for TE-ΦOTDR using SRDs to generate the optical frequency combs.

### 2.2. Comb generation

Figure 2(a) shows an example of the electrical pulses created by one of the SRD-based pulse generators when it is fed by a 10 MHz sinusoid. In this plot, the generated signal is digitized at a sampling rate of 10 GSa/s (blue dots) and the continuous curve (red line) is drawn by adding

Optics EXPRESS

values using a spline interpolation. The RF comb spectrum for a train of pulses with a duration of 5 ms (i.e., composed of $5 \times 10^4$ pulses) is shown in Fig. 2(b). As can be observed, it is a relatively flat-topped RF comb spanning 2 GHz, in accordance to the manufacturer's specifications [15]. A zoom-in view of 11 RF lines, located around 1.55 GHz, is displayed in Fig. 2(c). The line spacing of this spectrum can be precisely changed by simply choosing a different RF frequency to feed the SRD-based generator. The results shown in Fig. 2 are approximately replicated by the second diode used in our experimental setup. In principle, the time signal produced by the SRDs, when applied to a MZM set at its zero transmission point, gives rise to a spectrum in the optical domain with BW $\simeq$ 4 GHz (see next subsection), thus providing centimeter resolution if used as a probe for TE-φOTDR. By employing a method based on arbitrary waveform generation (for instance, by summing a set of cosines waves), an OFC with the above characteristics would require an ultrafast AWG able to produce a multi-tone signal composed of a frequency sequence covering the entire bandwidth [6,20].

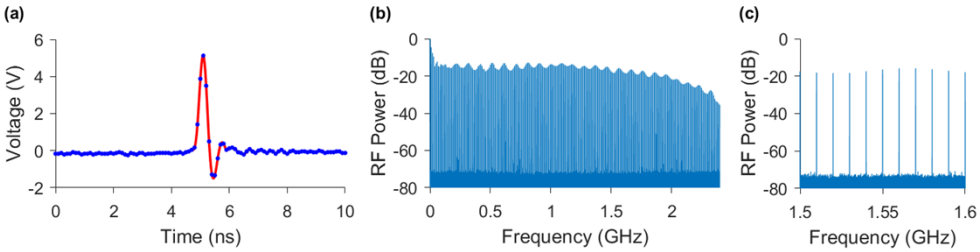


**Fig. 2.** (a) Electrical signal generated by one of the SRDs when is fed by a 10-MHz sinusoid. (b) Power spectra corresponding to a train of electrical pulses with a duration of 5 ms. (c) Magnified version of the spectrum showing the harmonics generated between 1.5 GHz and 1.6 GHz.

### 2.3. *Non-ambiguous frequency down-conversion*

When the laser light undergoes EO modulation, equally spaced spectral lines are originated around the optical frequency $\nu_0$. In accordance to the theory of dual-comb spectroscopy, the interference between the comb lines of the probe and the neighboring lines of the LO produces a RF comb with a line spacing equal to $\delta f$. If both OFC generators are directly fed by the laser, the generated spectra share the same central frequency $\nu_0$. As a consequence, pairs of lines symmetrically located with respect to $\nu_0$ originate beat notes exactly at the same frequency. To circumvent this ambiguity, the laser frequency in the LO arm is shifted by means of an AOFS, as is schematically depicted in Fig. 3. Then, the lines of the LO comb are created around $\nu_0 + f_{AO}$, where $f_{AO}$ is the RF frequency driving the AOFS, typically of the order of tens of megahertz and tunable within a small range around a central value. Since we consider $f_r \leq 10$ MHz (in order to achieve at least 10 m of sensing range), $f_{AO}$ can be chosen to be $f_{AO} = n_{AO} f_r + \Delta f$, where $n_{AO}$ is a positive integer and $\Delta f < f_r/2$. For the sake of clarity, Fig. 3 shows this particular selection when $n_{AO} = 1$. The shift of the entire LO comb with respect to the probe spectrum breaks the symmetry with respect to $\nu_0$ and makes each beat note to be located at a distinctive RF frequency. The result is the creation of a set of RF lines spaced by $\delta f$ and distributed around $\Delta f$ (with $\delta f \ll \Delta f$), which actually limits the impact of the $1/f$ noise. Depending on the value of $n_{AO}$, a small number of lines at the edges of the OFCs are filtered out in the down-conversion process due to the induced shift.

Optics EXPRESS

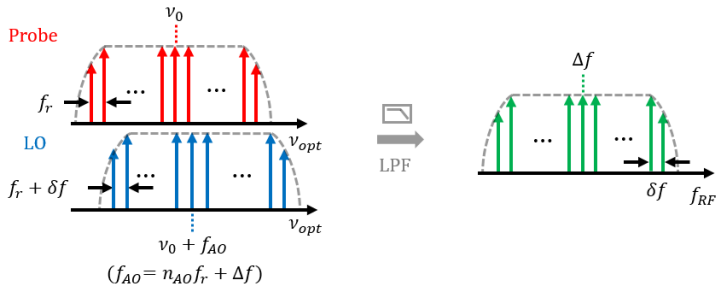


**Fig. 3.** Frequency-domain picture of the dual-comb scheme employed for TE-ΦOTDR. The interference between the probe OFC (red) and the frequency-shifted LO (blue) generates, after electrical low-pass filtering, a RF comb (green). In the plots, $\nu_{opt}$ ($f_{RF}$) stands for optical (RF) frequency.

### 2.4. Spatial resolution

In order to carry out TE-φOTDR, a couple of EO-OFCs with a high relative mutual coherence must be generated using the SRDs, so the interfering combs provide a set of well-defined narrow RF lines. To assess the performance of our dual-comb scheme, we configure the comb generators so $f_r = 10$ MHz, $\delta f = 50$ Hz and $f_{AO} = 82$ MHz ($n_{AO} = 8$, $\Delta f = 2$ MHz) . For this first measurement, the FUT is removed from the probe arm. Instead, we insert a variable attenuator to control the power of the light arriving at the second EDFA of that arm. The LPF has a cutoff frequency of 4 MHz. Figure 4(a) shows the RF spectrum around $\Delta f$ obtained from a 1-s signal composed of 50 IGMs with a duration of $T_{IGM} = 1/\delta f = 0.02$ s. The retrieved comb contains 400 lines for a power variation within 20 dB, which corresponds to 4 GHz of optical bandwidth. A magnified portion of the right side of this spectrum (around the 100$^{th}$ line) is shown in Fig. 4(b). We filter the RF comb (i.e., the part of the spectrum that is around $\Delta f$) and calculate the inverse Fast Fourier Transform (iFFT). The amplitude of the resulting signal is a train of peaks with a period equal to $T_{IGM}$ and a width that scales as the inverse of the spectral bandwidth. In accordance to the dual-comb theory, each peak is the result of the cross-correlation $c(t)$ between the probe and the LO electric fields [7], $c(t) = E^*_{LO}(-t) \otimes E_s(t)$, where $\otimes$ represents convolution, $*$ indicates the complex conjugate and the time $t$ is measured on an expanded scale defined by the factor $m = f_r/\delta f$. Figure 4(c) shows a zoom-in view of the correlation signal amplitude obtained by averaging over 50 consecutive peaks. Its full width at half maximum is $\delta t = (5.91 \pm 0.09) \times 10^{-5}$s. When the probe is launched into the FUT, every pulse is back-reflected from randomly distributed microscopic scattering centers. After processing the detected signal, we obtain the convolution $b(t)$ between the linear response $H(t)$ of the FUT and $c(t)$, $b(t) = c(t) \otimes H(t)$. The result is a noise-like trace with a phase that is sensitive to strain and temperature perturbations localized along the sensing fiber. By measuring phase changes in consecutive IGMs we can perform real-time sensing (see [6] for a more detailed description of TE-φOTDR). The position of a perturbation can be simply determined by writing the axial distance $z$ in terms of the light round-trip time $t' = t/m$ as $z = (1/2)\,(c/n)t'$. The spatial resolution $\delta z$ is then estimated as $\delta z = (1/2)\,(c/n)\,(\delta t/m)$. For our setup, $\delta z = 3$ cm (considering a conventional SMF-28 fiber).

Optics EXPRESS

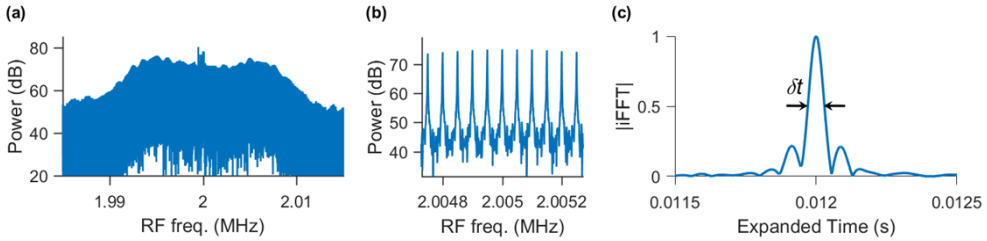


**Fig. 4.** (a) RF comb spectrum corresponding to the interference of the probe (without the FUT) and the LO. (b) Magnified view of the retrieved RF comb. (c) Normalized amplitude of the retrieved cross-correlation signal. The center of the peak is arbitrarily set within a fraction of the total expanded time window (equal to $1/\delta f$) of a single IGM.

## 3. Distributed sensing results

In our first sensing experiment, we insert a FUT ($L$ = 18 m) in the sample arm and configure our system so $f_r$ = 5 MHz, $f_{AO}$ = 82 MHz and $\delta f$ = 50 Hz. After retrieving the corresponding RF comb, we filter 800 lines around $\Delta f$ = 2 MHz and perform the iFFT. Figure 5 shows a set of consecutive traces obtained for this configuration. The SNR, calculated over 50 measurements, is 12 dB. A zoom-in view of a 2-m section of the trace can be observed in the upper inset, demonstrating good repeatability. To carry out sensing measurements, we use the shaker to stress the fiber along $PL$ = 4 cm at $z$ = 17.61 cm. The shaker is driven by a sinusoidal signal with a frequency of 5 Hz. We acquire a 1-s oscilloscope signal composed of 50 IGMs. For each one, we calculate the phase of the corresponding trace as a function of $z$. In fading points, the phase is estimated using a nearest neighbor analysis [21]. By applying a reconstruction algorithm (as described in [6]), we calculate the strain $\Delta\varepsilon$ induced by the shaker. The dynamic stress map of the perturbed area is shown in Fig. 6. The maximum strain variation is 1.24 με and the sensitivity of our system is 303 nε, which corresponds to a standard phase deviation of 0.14 rad.

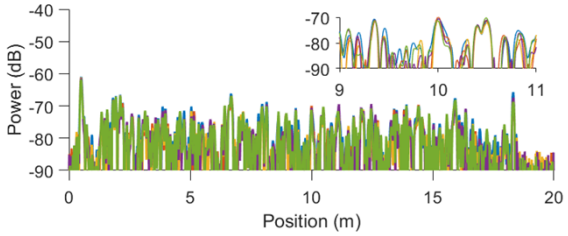


**Fig. 5.** Power of a set of detected traces for $\delta f$ = 50 Hz. A section of the FUT is shown in the upper inset to demonstrate the measurement repeatability.

In order to assess the dynamic response of our system, we set the acoustic sampling rate at $\delta f$ = 200 Hz. In this second experiment, the signal applied to the shaker has a frequency of 20 Hz and higher amplitude. Since increasing $\delta f$ implies a reduction in the SNR of the retrieved trace [6], we shorten the sensing length to 10 m. The disturbance is applied over $PL$ = 3 cm (the resolution limit) at the end of an 8-m fiber. The retrieved stress map $\Delta\varepsilon$ and the power spectral density (PSD) at the center of the perturbed section are shown in Fig. 7(a) and (b), respectively. In the PSD plot, we observe a well-defined peak at the perturbation frequency (20 Hz). Two harmonics are also detected in multiples of this frequency. These secondary peaks are explained by the nonlinear behavior of the shaker, which is clearly visible in Fig. 7 (a) (and also, although to a less extent, in Fig. 6). The maximum stress variation is now 5.6 με with a sensitivity of 320 nε. The PSD shows a noise floor of −25 dB ref.$1\mu\varepsilon^2$/Hz and the corresponding SNR (calculated

Optics EXPRESS

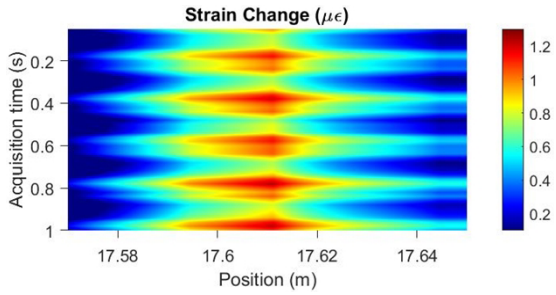


**Fig. 6.** Dynamic stress map around the perturbed section ($PL$ = 4 cm) using a dual-comb scheme with $f_r$ = 5 MHz (20 m of sensing range) and $\delta f$ = 50 Hz.

as the ratio between the signal peak and the noise floor) is 22 dB. The shaker employed in our experiments does not allow us to have a prior knowledge of the applied strain to the sensing fiber, in order to check the linearity between the demodulated phase signal and the induced strain variations. However, this analysis has been carried out experimentally in a previous demonstration of TE-φOTDR for temperature sensing, confirming a good linear behavior [6].

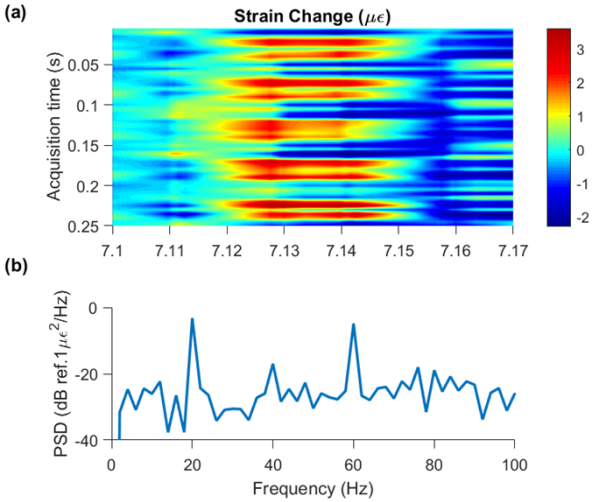


**Fig. 7.** (a) Dynamic stress map for $f_r$ = 10 MHz (10 m of sensing range), $\delta f$ = 200 Hz and $PL$ = 3 cm. (b) Power spectral density (PSD) at the perturbed section.

## 4. Discussion and conclusions

We have shown the capability to carry out TE-φOTDR using a couple of MZMs driven by SRDs. This approach allows us to avoid the requirement for exceptionally high-sampling-rate AWGs or the need of producing radiofrequencies of ~10 GHz with hertz precision. Specifically, we create OFCs with hundreds (up to 800) mutually coherent lines using a standard megahertz generator. As in any other dual-comb scheme, the efficient time expansion undergone by the signals generated after detection guarantees a digitization with low sampling rates (of tens of megahertz). The insertion of an AOFS to shift the laser wavelength in the LO arm enables us to employ the whole optical bandwidth and ensures a non-ambiguous down-conversion, in contrast to previous approaches for TE-φOTDR based on optical filtering. The availability of commercial SRD-based circuits providing flat-topped electrical spectra with gigahertz BWs ensures axial

Optics EXPRESS

resolutions of a few centimeters. The results obtained in this experiment were processed offline. However, fundamental parameters such as number of sensing points, trigger refresh rate and sampling rate, as well as the down-converted spectrum, are very similar to those reported in [17], where data processing was carried out in real time with the aid of a proper analog-to-digital converter card.

In principle, the sensing range can be expanded by decreasing the RF frequencies that feed the SRDs, thus reducing the repetition rate of the generated optical pulses. For a fixed optical bandwidth ($BW_{opt}$) and assuming a flat spectral phase, this implies an increase in the peak-to-average power ratio (PAPR) of the probe ($\sim BW_{opt}/f_r$) [8]. As in other φOTDR schemes that employ individual pulses, high PAPRs leads to a reduction in the average power of the probe signal to avoid the eventual onset of nonlinearities. In addition, the SRDs employed in our system produce electrical pulses with an amplitude that is drastically reduced for $f_r$<5 MHz (i.e., for sensing distances beyond 20 m), even when the maximum input power is applied to the diodes (+21 dBm). Therefore, the need to highly amplify the pulses to achieve driving amplitudes of around $V_\pi$ can easily provoke nonlinearities in the RF domain. Concerning the acoustic sampling rate, its maximum value is restricted by the requirement of locating all the RF lines (separated by $\delta f$) within the filtered detection BW. In accordance to this, $\delta f$ could be >1 kHz [7]. However, increasing $\delta f$ reduces the SNR of the recovered traces, as has been discussed in detail in [6], hence limiting the maximum measurement rate to a few hundreds of hertz.

The presented results show that our approach can offer easy implementation, reduced cost and high spatial resolution. However, in return, it exhibits a restricted performance in terms of sensing range and update rate when compared, under certain conditions, to previous TE-φOTDR demonstrations. If the proposed system is configured to obtain a sufficiently low PAPR (by adjusting $f_r$ while preserving a minimum SNR to recover the sensing information), the system will exploit all its sensing capabilities, reaching the maximum attainable acoustic sampling and completely filling the available RF spectrum. Then, no significant differences between the proposed scheme and those based on the use of an AWG will exist. On the contrary, higher PAPRs (such as in the case of considering a lower $f_r$ to expand the sensing range) entail a reduction in the SNR of the measured traces that is necessary to address. In schemes that employ an AWG, the strategy of coding the spectral phase reduces the PAPR, enabling an increase of the average power injected to the sensing fiber and, consequently, an improvement of the SNR. However, due to the impossibility of introducing such a codification in our combs, the SNR enhancement has to be performed through a reduction of the values of $\delta f$, as explained above. In particular, for the sensing performance shown in this article (centimeter resolution over a few tens of meters), the acoustic sampling is one order of magnitude lower than those reported in the AWG approaches [8]. On the other hand, the high centimeter resolution offered by our sensor is similar to that provided by optical frequency domain reflectometry (OFDR) sensors. In these systems, a swept-wavelength laser is combined with a heterodyne detection system, so each measured beat frequency is directly related to a particular location along the sensing range. The spatial resolution is simply given by the inverse of the frequency range covered during a complete sweep. Nevertheless, such a theoretical operation is seriously degraded by the existence of sweep nonlinearities. This drawback is usually overcome by including an auxiliary interferometer in the OFDR system to measure the instantaneous optical frequency. This enables a precise correction of the frequency sampling using an interpolation algorithm [22], although at the expense of significantly increasing the data processing and the complexity of the sensor architecture.

In conclusion, the proposed system is an inexpensive and easily implementable solution for TE-φOTDR over distances of tens of meters, with a global performance that can compete with other distributed sensing technologies in terms of resolution and speed (see, for instance, the comparative analysis in [17]). The use of standard optical fibers, along with the above features, highlights the real capabilities of the proposed dual-comb system for high spatial resolution

Optics EXPRESS

distributed measurements. As a result, our approach is especially suitable for engineering applications that also require a moderate speed, becoming a cost-efficient alternative to frequency-domain methods [18,19]. Besides, further developments to circumvent the use of high-end AWGs are still possible. By a proper design, it is possible to optimize the performance of SRD-based circuits [23], particularly to overcome amplitude limitations [24,25]. Following a different strategy, multi-stage OFC generators [26] could be adapted to the requirements demanded by high-resolution φOTDR. This would provide an alternative option to improve the sensor capabilities, but at the obvious cost of a more sophisticated dual-comb architecture.

**Funding.** Comunidad de Madrid/FEDER Program (SINFOTON2-CM: S2018/NMT-4326); Generalitat Valenciana (PROMETEO/2020/029); Universitat Jaume I (UJI-B2019-45); European Union Next Generation EU/PRTR Program (PSI ref. PLEC2021-007875, TREMORS ref. CPP2021-008869); MCIN/AEI/10.13039/501100011033/ "FEDER A way of making Europe" (PID2021-124814NB-C22, PID2021-128000OB-C21, PID2021-128000OB-C22, RTI2018–097957-B-C31, RTI2018–097957-B-C32, RTI2018–097957-B-C33); HORIZON EUROPE European Innovation Council (Ref.101098992).

**Acknowledgments.** The work of Miguel Soriano-Amat and Vicente Durán was supported in part by MCIN/AEI/ 10.13039/ 501100011033 and "ESF Investing in your future" under grants PRE-2019-087444 and RYC-2017-23668, respectively. The work of María R. Fernández-Ruiz was supported by the MCIN/AEI/ 10.13039/ 501100011033 under grant IJC2018–035684-I. This publication is part of the project PID2021-124814NB-C22, funded by MCIN/AEI/10.13039/501100011033/ "FEDER A way of making Europe".

**Disclosures.** The authors declare no conflicts of interest.

**Data Availability.** The data underlying the results presented in this paper are not publicly available at this time but may be obtained from the authors upon reasonable request.

## References

1. J. C. Juarez, E. W. Maier, K. N. Choi, and H. F. Taylor, "Distributed fiber-optic intrusion sensor system," J. Lightwave Technol. **23**(6), 2081–2087 (2005).
2. Y. Lu, T. Zhu, L. Chen, and X. Bao, "Distributed vibration sensor based on coherent detection of phase-OTDR," J. Light. Technol. **28**(22), 3243–3249 (2010).
3. P. Lu, N. Lalam, M. Badar, B. Liu, B. T. Chorpening, M. P. Buric, and P. R. Ohodnicki, "Distributed optical fiber sensing: Review and perspective," Appl. Phys. Rev. **6**(4), 041302 (2019).
4. M. D. Jones, "Using Simplex Codes to Improve OTDR Sensitivity," IEEE Photon. Technol. Lett. **5**(7), 822–824 (1993).
5. D. Lee, H. Yoon, P. Kim, J. Park, and N. Park, "Optimization of SNR improvement in the noncoherent OTDR based on simplex codes," J. Lightwave Technol. **24**(1), 322–328 (2006).
6. M. Soriano-Amat, H. F. Martins, V. Durán, L. Costa, S. Martin-Lopez, M. Gonzalez-Herraez, and M. R. Fernández-Ruiz, "Time-expanded phase-sensitive optical time-domain reflectometry," Light: Sci. Appl. **10**(1), 51 (2021).
7. N. R. Newbury, I. Coddington, and W. Swann, "Sensitivity of coherent dual-comb spectroscopy," Opt. Express **18**(8), 7929–7945 (2010).
8. M. Soriano-Amat, H. F. Martins, V. Durán, S. Martin-Lopez, M. Gonzalez-Herraez, and M. R. Fernández-Ruiz, "Quadratic phase coding for SNR improvement in time-expanded phase-sensitive OTDR," Opt. Lett. **46**(17), 4406–4409 (2021).
9. J. Preciado-Garbayo, M. Soriano-Amat, P. Sevillano, D. Izquierdo, H. F. Martins, S. Martin- Lopez, M. Gonzalez-Herraez, M. R. Fernández-Ruiz, and J. J. Martínez, "Time-Expanded-OTDR based on binary sequences," IEEE Photon. Technol. Lett. **34**(13), 695–698 (2022).
10. H. T. Friis, "Analysis of Harmonic Generator Circuits for Step Recovery Diodes," Proc. IEEE **55**(7), 1192–1194 (1967).
11. J. L. Moll and S. A. Hamilton, "Physical Modeling of the Step Recovery Diode for Pulse and Harmonic Generation Circuits," Proc. IEEE **57**(7), 1250–1259 (1969).
12. T. Sakamoto, I. Morohashi, T. Kawanishi, and I. Hosako, "Picosecond pulse generation using low-driving-voltage MZM driven with step recovery diodes," in *CLEO/Europe - EQEC 2009 - European Conference on Lasers and Electro-Optics and the European Quantum Electronics Conference*, 2009, paper JWA36.
13. A. Rosado, E. P. Martin, A. Pérez-Serrano, J. Manuel, G. Tijero, I. Esquivias, and P. M. Anandarajah, "Optical frequency comb generation via pulsed gain-switching in externally- injected semiconductor lasers using step-recovery diodes," Opt. Laser Technol. **131**, 106392 (2020).
14. A. J. Fleisher, D. A. Long, Z. D. Reed, J. T. Hodges, and F. Plusquellic, "Coherent cavity-enhanced dual-comb spectroscopy," Opt. Express **24**(10), 10424–10434 (2016).
15. "TBCG2 Comb generator/ Frequency multiplier." [Online]. Available: https://www.tekbox.com/.

Optics EXPRESS

16. D. A. Long, A. J. Fleisher, K. O. Douglass, S. E. Maxwell, K. Bielska, J. T. Hodges, and D. F. Plusquellic, "Multiheterodyne spectroscopy with optical frequency combs generated from a continuous-wave laser," Opt. Lett. **39**(9), 2688–2690 (2014).
17. M. Soriano-Amat, D. Fragas-Sánchez, H. F. Martins, D. Vallespín-Fontcuberta, J. Preciado-Garbayo, S. Martin-Lopez, M. Gonzalez-Herraez, and M. R. Fernández-Ruiz, "Monitoring of a highly flexible aircraft model wing using time-expanded phase-sensitive OTDR," Sensors **21**(11), 3766 (2021).
18. S. M. Klute, A. K. Sang, D. K. Gifford, and M. . Froggatt, "Defect detection during manufacture of composite windturbine blade with embedded fiber optic distributed strain sensor," in *Proceedings of the International SAMPE Technical Conference, Long Beach, CA, USA*, 23–26 May 2011.
19. N. A. Rahim, J. Kutz, M. White, J. Michel, A. Sang, M. Froggatt, S. Klute, and D. Gifford, "Dynamic monitoring of fan blade using high resolution, distributed fiber optic sensing," in *Proceedings of the SAMPE Technical Conference, Wichita, KS, USA*, 21–24 October 2013.
20. M. Soriano-Amat, M. A. Soto, V. Duran, H. F. Martins, S. Martin-Lopez, M. Gonzalez-Herraez, and M. R. Fernández-Ruiz, "Common-Path Dual-Comb Spectroscopy Using a Single Electro-Optic Modulator," J. Lightwave Technol. **38**(18), 5107–5115 (2020).
21. G. Tu, M. Zhao, Z. Tang, K. Qian, and B. Yu, "Fading noise suppression in Φ-OTDR based on nearest neighbor analysis," J. Lightwave Technol. **38**(23), 6691–6698 (2020).
22. J. Li, J. Gan, Z. Zhang, X. Heng, C. Yang, Q. Qian, S. Xu, and Z. Yang, "High spatial resolution distributed fiber strain sensor based on phase-OFDR," Opt. Express **25**(22), 27913–27922 (2017).
23. J. Han and C. Nguyen, "Ultra-Wideband Electronically Tunable Pulse Generators," IEEE Microw. Wireless Compon. Lett. **14**(3), 112–114 (2004).
24. A. Kheirdoost, G. Moradi, E. Elkholy, A. Abdipour, and A. E. Fathy, "Modeling and jitter improvement of SRD-based ultra-wideband pulse generator," IEEE Trans. Microwave Theory Tech. **62**(8), 1736–1747 (2014).
25. R. Feghhi, R. Winter, and K. Rambabu, "A High-Performance UWB Gaussian Pulse Generator: Analysis and Design," IEEE Trans. Microwave Theory Tech. **70**(6), 3257–3268 (2022).
26. B. Xu, X. Fan, S. Wang, and Z. He, "Broadband and high-resolution electro-optic dual-comb interferometer with frequency agility," Opt. Express **27**(6), 9266–9275 (2019).